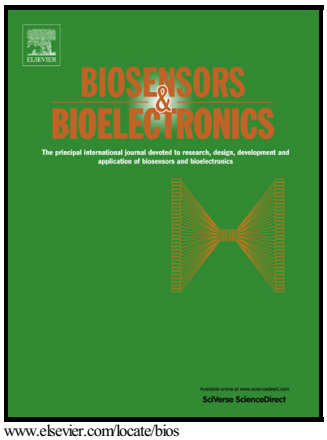

www.elsevier.com/locate/bios

Real-time electrochemical detection of Hydrogen peroxide secretion in live cells by Pt nanoparticles Decorated graphene–carbon nanotube Hybrid paper electrode

Yimin Sun, Kui He, Zefen Zhang, Aijun Zhou, Hongwei Duan

PII: S0956-5663(15)00018-4
DOI: http://dx.doi.org/10.1016/j.bios.2015.01.017
Reference: BIOS7392

To appear in: *Biosensors and Bioelectronic*

Received date: 29 October 2014
Revised date: 26 December 2014
Accepted date: 7 January 2015

Cite this article as: Yimin Sun, Kui He, Zefen Zhang, Aijun Zhou and Hongwei Duan, Real-time electrochemical detection of Hydrogen peroxide secretion in live cells by Pt nanoparticles Decorated graphene–carbon nanotube Hybrid paper electrode, *Biosensors and Bioelectronic,* http://dx.doi.org/10.1016/j.bios.2015.01.017

Real-time electrochemical detection of hydrogen peroxide secretion in live cells by Pt nanoparticles decorated graphene–carbon nanotube hybrid paper electrode

Yimin Sun[a,b], Kui He[a], Zefen Zhang[a], Aijun Zhou[a,*], Hongwei Duan[b,*]

[a] *School of Material Science and Engineering, Wuhan Institute of Technology, Wuhan, Hubei 430073, People's Republic of China*

[b] *School of Chemical and Biomedical Engineering, Nanyang Technological University, 70 Nanyang Drive 637457, Singapore*

Abstract

In this work, we develop a new type of flexible and lightweight electrode based on highly dense Pt nanoparticles decorated free-standing graphene–carbon nanotube (CNT) hybrid paper (Pt/graphene–CNT paper), and explore its practical application as flexible electrochemical biosensor for the real-time tracking hydrogen peroxide (H_2O_2) secretion by live cells. For the fabrication of flexible nanohybrid electrode, the incorporation of CNT in graphene paper not only improves the electrical conductivity and the mechanical strength of graphene paper, but also increases its surface roughness and provides more nucleation sites for metal nanoparticles. Ultrafine Pt nanoparticles are further decorated on graphene–CNT paper by well controlled sputter deposition method, which offers several advantages such as defined particle size and dispersion, high loading density and strong adhesion between the nanoparticles and the substrate. Consequently, the resultant flexible Pt/graphene–CNT paper electrode demonstrates a variety of desirable electrochemical properties including large electrochemical active surface area, excellent electrocatalytic activity, high stability and exceptional flexibility. When used for nonenzymatic detection of H_2O_2,

Corresponding author. Tel.: +86 27 87195661; Fax: +86 27 87195661, E-mail address: zhouaijun3@sina.com (A. Zhou), hduan@ntu.edu.sg (H. Duan).

Pt/graphene–CNT paper exhibits outstanding sensing performance such as high sensitivity, selectivity, stability and reproducibility. The sensitivity is 1.41 μA μM^{-1} cm^{-2} with a linear range up to 25 μM and a low detection limit of 10 nM (S/N = 3), which enables the resultant biosensor for the real-time tracking H_2O_2 secretion by live cells macrophages.

Keywords: Graphene–carbon nanotube hybrid paper; Pt nanoparticles; Sputter deposition; Flexible electrochemical biosensor; Nonenzymatic hydrogen peroxide detection; Cell tracking

1. Introduction

The integration of nanoscale building blocks into macroscopic level by self-assembly method has been recognized as one of the most effective strategies to realize the practical applications of nanomaterials (Tang et al., 2010). Nowadays, remarkable progress has been made in self-assembly of carbon materials into two-dimensional (2D) forms such as graphite foil, carbon paper and buckypaper (Endo et al., 2005). Graphene, the latest allotrope of carbon following fullerenes and carbon nanotubes, has intrigued great attentions for their unique properties including high electrical conductivity, huge specific surface area, high charge carrier mobility and mechanical flexibility (Ensafi et al., 2014; Lee et al., 2008; Nair et al., 2008; Novoselov et al., 2004; Sun et al., 2011). Recent studies including us have shown that graphene oxides (GO) or graphene nanosheets dispersed in water or in hydrosol form can also be assembled into a macroscopic well-ordered paper-like structure (Chen et al., 2008; Dikin et al., 2007; Park et al., 2010; Pei et al.,2010; Xiao et al., 2012; Yang and Zou, 2014). The as-prepared graphene papers display a combination of exceptional thermal, mechanical, and electrical properties, which are superior to other carbon-based paper materials. These enable graphene paper a promising candidate in a broad spectrum of applications ranging from supercapacitors, Li-ion batteries to bioengineering and super adsorbents (Chi et al., 2014; Gao et al., 2012; Hu et al.,

2013; Li et al., 2012; Oh et al., 2014; Wang et al., 2009). However, it is still a challenge to extend its application to high-performance flexible electrode for electrocatalysis because of the limited surface area of the 2D graphene paper, the insufficient active sites for anchoring electrocatalytic metal nanoparticles, and the lack of effective strategy to deposit metal nanoparticles with high loading density and strong adhesion with the substrates.

In this work, we developed a new type of flexible and light-weight nanohybrid paper based on ultrafine Pt nanoparticles decorated free-standing graphene–carbon nanotube (CNT) paper. The incorporation of CNT into graphene paper not only prevents the agglomeration between each other of graphene nanosheets (Shakir, 2014), but also improves the electrical conductivity and the mechanical strength of graphene paper, as well as increases the surface roughness and provides more nucleation sites for metal nanoparticles. The graphene–CNT paper can further be functionalized with Pt nanoparticles by a well-developed sputter deposition process, which can efficiently avoid the formation of large metal particles because of the high surface free energy of metal atoms, leading to the formation of metal nanoparticles with defined size and distribution, high loading density and strong adhesion between the nanoparticles and the substrate (Hobbs et al., 2004; Kashem et al., 2011; You et al., 2002).

Taking the advantages of the free-standing graphene–CNT paper as well as the sputter-deposited Pt nanoparticles on it, the obtained Pt nanoparticles decorated graphene–CNT (Pt/graphene–CNT) paper electrode exhibits large electrochemical active surface area, excellent electrocatalytic activity, high stability and distinctive flexibility, which enable it to be used as flexible electrochemical biosensor for the real-time tracking hydrogen peroxide (H_2O_2) secretion by live cells. H_2O_2 is produced by almost all oxidases in mitochondria and can diffuse out freely through membranes to reach various cellular compartments. Developing a quantitative assay of H_2O_2 in biological solutions is of great importance in chemical industry, pharmaceutical, biology, biomedicine diagnosis, food processing and environment monitoring (Chen et al., 2012; Guascito et al., 2011; Han et al., 2013; Ji et al., 2011; Miao et al., 2013;

Liu et al., 2013; Suárez et al., 2013; Sun et al., 2012; Xi et al., 2013.; Xiao et al., 2009; Xu et al., 2011). When used for nonenzymatic detection of H_2O_2, Pt/graphene–CNT paper exhibits good sensing performances such as high sensitivity, selectivity, stability and reproducibility. The resultant biosensor shows a high sensitivity of 1.41 μA μM^{-1} cm^{-2} with a linear range up to 25 μM and a low detection limit of 10 nM (S/N = 3), and can be used for the real-time tracking H_2O_2 secretion by live cells macrophages, demonstrating its promising application for in-vivo and in-vitro clinical diagnostics. All these outstanding features make the free-standing flexible and lightweight paper electrode an intriguing candidate for the development of high-performance sensor units for practical applications in fields of point-of-care testing instruments, implantable/ wearable medical devices and microscale biosensor for physiological and pathological investigations.

2. Experimental

2.1. Preparation of nanohybrid paper electrodes

The graphene oxide was firstly synthesized from graphite powder based on a modified Hummers method (Hummers and Offeman, 1958). The exfoliation of graphene oxide (GO) nanosheets was achieved by ultrasonication of the dispersion for 2 h. The as-obtained GO samples were washed with distilled water and dried under vacuum. Multi-walled CNTs (10~20 nm in diameter, 10~30 μm in length, 95%, 200~350 m^2 g^{-1}) were purchased from Nanostructured & Amorphous Materials Inc. (USA). Before using, CNTs were pretreated by refluxing in HNO_3-H_2SO_4 (v/v, 1:1) mixture for 2 h at 55 °C and then for 3 h at 80 °C, washed with redistilled water and dried under vacuum. GO and purified CNTs were mixed and dispersed into distilled water to form a uniform black suspension, with different ratio of GO to CNTs (i.e., 9:1, 4:1, 3:1, 2:1 and 1:1). The GO–CNT paper was prepared by evaporation-assisted self-assembly process. In details, the aqueous dispersion of GO–CNT nanocomposite was placed in a casting mold made of polyethylene terephthalate (PET). After water was completely removed through slow evaporation at room temperature for 24 h, the

freestanding GO–CNT paper can be easily peeled off from PET matrix. Reduced GO (rGO)–CNT paper was prepared by chemical reduction of GO–CNT paper. In a typical procedure, GO–CNT paper was directly immersed into hydroiodic acid (HI) solution in a sealed cuvette at room temperature for 1 h. The HI-reduced GO–CNT paper was washed with DI water for several times. After dried at room temperature for 10 h, the rGO–CNT paper was obtained. For comparison, rGO paper was also prepared under the same procedure condition according to our previous work (Xiao et al., 2012). The sputter deposition of Pt nanoparticles on rGO–CNT paper was performed by vacuum sputter coating machine. The deposition time was 300 s and the current was 20 mA. The as-prepared electrode was denoted as Pt/rGO–CNT paper. Pt/rGO paper was prepared through a similar method.

2.2. Characterization and electrochemical measurement

Scanning electron microscope (SEM) image was obtained using JEOL field-emission scanning electron microscope (JSM-6700F), equipped to perform elemental chemical analysis by energy dispersive X-ray spectroscopy (EDX). Sputter deposition was carried out with JFC-1600 Auto fine coater (Japan). Cyclic voltammetric (CV) and chronoamperometric (CA) experiments were performed with a CHI 660 D electrochemical workstation (CH Instrument Company). During the electrochemical measurements, the working electrode was a contacted nanohybrid paper electrode set in cell device, and the auxiliary and reference electrodes were Pt wire and Ag/AgCl, respectively.

3. Results and discussion

3.1. Physicochemical characterization of different nanohybrid papers

The graphene–CNT paper used in this study has been prepared by evaporating the mixture of exfoliated GO nanosheets and CNTs in casting molds, and then converted to rGO–CNT paper by chemical reduction using HI as the reducing reagents. The as-obtained flexible rGO–CNT paper is black in colour and lacklustre on both sides, different from pure rGO paper that exhibits a shining metallic lustre (Inset of Fig. 1).

The obtained rGO–CNT paper exhibits light weight of 1.0 mg cm^{-2} and excellent mechanical flexibility. Its tensile strength reaches 109.6 MPa with an ultimate tensile strain of 9.21 % (Fig. 1), which are superior to those of the pure rGO paper (Li et al, 2012), and more detailed data are shown in Supporting Information (Table S1). Since the CNTs are elastic regardless of their being straight or coiled, the CNTs inside the graphene paper are considered to be cushioning, and the rGO–CNT paper is therefore more strong and elastic in mechanics than pure rGO paper. In this work, the ratio of GO to CNTs in rGO–CNT paper has also been optimized. Our results have demonstrated that along with increased ratio of GO to CNTs from 9:1 to 2:1, the mechanical strength and surface roughness also increase dramatically. However, when the ratio of GO to CNTs exceeds 2:1, the mechanical strength of the rGO–CNT paper trends to decrease. As for 1:1 ratio of GO to CNTs, rGO–CNT paper becomes too brittle because of the formation of loose structure with low content of GO in paper, as shown in Supplementary Materials (Fig. S1). Furthermore, the composite of GO and CNTs with lower ratio of GO to CNTs cannot form free-standing paper structure by the proposed evaporation-assisted self-assembly process. Taking all these into account, we choose the rGO–CNT paper with the optimal ratio of 2:1 for the following experiments.

Figure 1

The microscopic morphology of rGO–CNT paper was characterized by SEM. Fig. 2A and 2B show that the rGO–CNT paper demonstrates a typical layer by layer structure throughout the entire cross-section with a thickness of 10 μm (Fig. S1), meanwhile, the rGO layers are regularly spaced by the incorporated CNT. The top-section SEM images reveal that rGO–CNT paper exhibits a rough corrugated surface feature, where the CNTs with a diameter of ~15 nm are uniformly distributed on the whole surface (Fig. 2C and 2D). Although the pure rGO paper also exhibits a layered structure throughout its cross-section area and a wrinkled texture associated with flexible nature of graphene nanosheets (Fig. 2E and 2F), its top surface is much

smoother than that of rGO–CNT paper. For rGO–CNT paper, the intercalation and distribution of highly conductive CNTs between the graphene sheets not only increase the surface roughness and also improve the electrical connectivity between the graphene nanosheets and CNTs. The conductivity of rGO–CNT paper is estimated to be about 6340 S m^{-1} at room temperature, which is higher than that of rGO paper (5150 S m^{-1}). These characteristics make rGO–CNT paper a highly desirable electrode material for various electrochemical applications.

Figure 2

Nanostructured Pt catalyst was decorated on rGO–CNT paper and rGO paper by sputter deposition method. After sputtering, the surfaces of rGO–CNT and rGO papers are entirely covered by a layer of ultrafine Pt nanoparticles, and resultant Pt/rGO–CNT and Pt/rGO papers exhibit a rough texture of the sandy desert surface (Fig. 3A and 3D). The Pt layer is fairly thin so that the morphological characteristics of graphene nanosheets and CNTs are still visible (Fig. 3B and 3E). The enlarged view reveals that Pt particles decorated rGO–CNT paper and rGO paper surface have uniform nanometer-size of 10~15 nm and ordered metal nanostructures (Fig. 3C and 3F). These nanoparticles are closely packed and uniformly distributed on the paper surface with high loading density, and no aggregation of particles has been observed on both rGO–CNT paper and rGO paper, which is benefit from the sputter deposition pathway that provides good control over particle size and size distribution, which make the resultant nanohybrid paper function as Pt-based nanostructured electrode material for electrocatalysis application (Chen and Holt-Hindle, 2010).

Figure 3

3.2. Electrochemical characterization of different nanohybrid papers

The electrochemical characteristics of different nanohybrid paper electrodes are studied using $Fe(CN)_6^{3-/4-}$ as the redox probe. As reflected by CV curves that both of rGO-CNT paper and rGO paper exhibits a pair of quasi-reversible Faradic currents

associated with the well-defined redox waves of the $Fe(CN)_6^{3-/4-}$ couple, however, the Faradic current as well as the capacitive current of rGO-CNT paper are much larger than those of pristine rGO paper (Fig. 4A), suggestive of an increased specific surface area and double layer capacitance of rGO–CNT paper. This can be attributed to the intercalation of CNTs between the graphene sheets, which restricts the restacking of graphene nanosheets and increases the specific surface area of the graphene paper electrode. More importantly, our results demonstrate that upon being coated by a layer of Pt nanoparticles, the peak currents of Pt/rGO–CNT paper and Pt/rGO paper dramatically increase with respect to those of rGO–CNT paper and rGO paper, in accompany with a decreased peak potential separation, which demonstrates that the decoration of Pt nanoparticles on the surface of graphene-based paper materials significantly increases the electroactive surface area as well as accelerates the electron transfer between the electrode and the redox species in solution. Furthermore, the peak currents of Pt/rGO–CNT paper are found to be much larger than those of Pt/rGO paper, signifying that the rGO–CNT paper with larger surface area and more nucleation sites is a superior substrate to support electroactive nanomaterials.

The CV curves of Pt/rGO–CNT paper and Pt/rGO paper with commercial Pt foil as control in deaerated 0.5 M H_2SO_4 solution depict that the hydrogen monolayer adsorption/desorption peaks from -0.2 V to 0.1 V and the characterized Pt oxide formation/stripping peak at 0.5 V of polycrystalline bulk Pt are readily seen (Fig. 4B). The electrochemically active surface areas (ECSA) of individual electrode can be estimated by the cathodic or anodic charge in the hydrogen adsorption/desorption region (Seger and Kamat, 2009). According to the calculation, Pt/rGO–CNT paper has a high ECSA up to 57.3 $m^2\ g^{-1}$, which is over 40% increase relative to that of Pt/rGO paper (40.2 $m^2\ g^{-1}$) and about 16-folds increase relative to that of Pt foil (3.6 $m^2\ g^{-1}$), further confirming that rGO–CNT paper provides larger surface area for loading nanocatalyst, which to a great extent increase the ECSA. EDX analysis has been performed to estimate the Pt content in the hybrid paper (Fig. 4C inset), which shows that the ECSA of the hybrid paper increase with Pt content. However, when the

Pt content exceeds 40%, the ECSA trends to decrease (Fig. 4C), probably due to the aggregation of Pt nanoparticles on the surface of the paper. The stability testing shows that the Pt/rGO–CNT paper loses less than 10% of its initial ECSA after 1000 cycles in 0.5 M H_2SO_4 solution (Fig. 4D), demonstrating a strong anchor of Pt on the rGO-CNT paper by sputter deposition process.

Figure 4

3.3. Electrochemical sensing performance of Pt/rGO–CNT paper

The electrochemical sensing performances of different paper electrode have been investigated in 0.1 M phosphate buffer solution (PBS, pH 7.4) containing 1.0 mM H_2O_2. Fig. 5A displays CVs of Pt/rGO–CNT paper electrode and Pt foil electrode at a scan rate of 50 mV s^{-1}. Pt/rGO–CNT paper exhibits a distinct reduction current towards the electrochemical reduction of H_2O_2 with respect to that of Pt foil, indicative of higher activity for H_2O_2 reduction on Pt/rGO–CNT paper. Moreover, the amperometric signals of H_2O_2 on both Pt/rGO–CNT paper and Pt foil electrodes at different applied detection potentials are shown in Fig. 5B. The results demonstrate that Pt foil electrode exhibits highest current density towards the reduction of H_2O_2 at a negative potential of -0.25 V. When the applied detection potentials shift to positive values, the electrochemical response of H_2O_2 decreases dramatically. For comparison, the reduction current of H_2O_2 reach maximum value at about -0.05 V for Pt/rGO–CNT paper electrode, and the amperometric current density is much higher than that of Pt foil. Benefit from the selected potential of -0.05 V for the electrochemical reduction of H_2O_2, Pt/rGO–CNT paper electrode is free from the common interferences that normally co-exists with H_2O_2 in biological systems, such as oxygen, ascorbic acid (AA), uric acid (UA), dopamine (DA), xanthine, adenine, cytosine, guanine and thymine, K^+, Ca^{2+}, Ni^{2+}, Na^+, Mg^{2+}, Al^{3+}, Zn^{2+}, Fe^{2+}, Co^{2+}, Ni, Cl^-, NO_2^-, NO_3^-, SO_4^{2-}, ClO_4^-, CO_3^{2-}, PO_4^{3-} (Table S2), suggestive of it high selectivity for electrochemical sensing of H_2O_2.

Fig. 5C depicts the amperometric responses of Pt/rGO–CNT paper electrode along with control Pt/rGO paper electrode in the presence of 1.0, 2.0, 5.0 and 10 μM H_2O_2 in 0.1 mM PBS (pH 7.4). Pt/rGO–CNT paper electrode displays sensitive amperometric responses for successive addition of H_2O_2 (Fig. 5C inset), and the current densities of H_2O_2 on Pt/rGO–CNT paper electrode are almost two times higher than those on Pt/rGO paper electrode. Nevertheless, there is not any distinct redox peaks of H_2O_2 observed on rGO–CNT paper and rGO paper electrodes, indicating that the high electrocatalytic activity is attributed to the highly dense Pt nanoparticles that decorated on graphene paper. The probable electrocatalytic mechanism of H_2O_2 redox at Pt-based electrode involves Pt/Pt(II) electroactive redox pairs, which could be responsible for the electrochemical and/or the catalytic dissociation of H_2O_2 (Guascito et al., 2011). Moreover, upon each addition of H_2O_2, the response of Pt/rGO–CNT paper electrode rapidly reaches 95% of the steady-state value within 3 s (Fig. 5D). A good linear dependence on the H_2O_2 concentration in the range of 0.1~25 μM can be achieved, with a sensitivity of 1.41 μA cm^{-2} μM^{-1} and a detection limit down to 10 nM at a signal-to-noise (S/N) ratio of 3 (Fig. 5E). The sensing performances of sensitivity, linear range and detection limit obtained with the proposed flexible sensor are comparable or even superior to those of the previously reported electrochemical sensors for the determination of H_2O_2 (Table S3).

Taking into account that the flexibility is of great importance for the practical application of flexible biosensor device (Chuang et al., 2010; Wu et al., 2010), the influences of the bending-induced mechanical stress on the overall sensing performance of Pt/rGO–CNT paper electrode have been investigated. After 180° bending for 500 times, the changes of amperometric responses to 5.0 μM H_2O_2 are less than 10 %. Additionally, upon bending inward to angles of 45°, 90° and 180°, the changes of the amperometric response towards 5.0 μM H_2O_2 are negligible. The reproducibility and repeatability of the flexible electrodes are further evaluated. The results shows that the relative standard deviation (RSD) values of amperometric response for eight different Pt/rGO–CNT paper electrode are less than 5% (Fig. 5F).

The catalytic current response can maintain over 90% of its initial value even after three month. These reflect the excellent mechanical strength, reproducibility and stability of the Pt/rGO–CNT paper electrode.

Figure 5

3.4. Detection of H_2O_2 released by live cells macrophage

Owing to the excellent sensing performance of Pt/rGO–CNT paper electrode, it can be used for *in vitro* and *in vivo* H_2O_2 detection. In this work, Pt/rGO–CNT paper electrode has been employed for real-time tracking H_2O_2 secretion by live cells macrophages, which play an important role in host defence against various microbes as well as tumors (Dong et al., 2014). To detect the secretion of H_2O_2 by live cell, the cells were grown in a 24-well plate to 80% confluency in 0.1 M PBS (pH 7.4), the cell number is 3×10^5, which were stimulated to release H_2O_2 by phorbol 12-myristate-13-acetate (PMA). Cytotoxicity of the Pt/rGO–CNT paper was evaluated using a standard cell counting Kit-8 (CCK-8) assay in a 96-well plate. One piece of Pt/rGO–CNT paper was added into every well tested and incubated with cells for 0~4 h. Afterward, CCK-8 solutions were added to each tested wells, and the absorbance of every well at 450 nm was measured using a microplate reader after 4 h incubation. As shown in Fig. 6A and 6B, the cells incubated with the Pt/rGO–CNT paper electrode for over 4 h were very healthy. The cell viability was calculated based on the ratio of the absorbance of the sample well to that of the control cell and expressed as a percentage, which maintained ~90% viability after 4 h incubation with the paper electrode (Fig. 6C).

To detect the secretion of H_2O_2 by live cell, a conventional three-electrode system was adopted for the electrochemical experiments, with the graphene paper (1 cm × 0.5 cm) as the working electrode. Upon the addition of 0.1 mM PMA, the current response of Pt/rGO–CNT paper electrode dramatically increases to 1.15 μA cm^{-2} for macrophage within 12 s, which further decreases down to the level of background signal after addition of a H_2O_2 scavenger catalase. Control wells containing no macrophages do not generate any response towards the addition of

equal amount of PMA (Fig. 6D). These indicate that the generated increase of amperometric responses is ascribed to the electrochemical reduction of H_2O_2 released by live cells upon being stimulated by PMA.

The reproducibility and stability have been investigated by using Pt/rGO–CNT paper electrode for the real-time detection of H_2O_2 secretion in six different 24-well plates with the same number of macrophages. The results demonstrate that the RSD values of the increased amperometric responses and the response times to reach the plateau for macrophages upon the addition of 0.1 mM PMA in six different 24-well plates are less than 10%, and the average current density and the response time are 0.87 μA cm^{-2} and 23 s, respectively (Fig. S3), Furthermore, in order to investigate the dependence of sensor's response on the cell number, we have performed an experiment of varying the cell number, using the macrophages cells with number of 3×10^5, 6×10^4 and 8×10^3. The results reveal that upon the addition of equal amount of PMA, the increase amperometric current densities of the released H_2O_2 for 3×10^5, 6×10^4 and 8×10^3 cells are 0.87, 0.43 and 0.25 μA cm^{-2}, respectively. This indicates that the amount of the peroxide release increases with the increase of cell number. However, the response time to reach the plateau is independent on the number of cells. Additionally, the reaction rate for scavenging H_2O_2 by catalase is a constant value of about 17.8 nM s^{-1}. These observations substantially demonstrate the potential of the proposed flexible sensor for the reliable qualitative and semi-quantitative determination of H_2O_2 secreted by live cells, which will be very promising for further physiological and pathological investigations.

Figure 6

4. Conclusions

In summary, we developed a facile and effective method to fabricate a new type of flexible and lightweight electrode based on the sputter deposition of ultrafine Pt nanoparticles on free-standing rGO–CNT paper. Owing to the synergistic effect of different components in the Pt/rGO–CNT paper, the resultant nanohybrid paper

exhibited excellent mechanical, physicochemical and electrochemical properties. When used as a freestanding paper electrode for flexible electrochemical biosensor, the Pt/rGO–CNT electrode demonstrated a remarkably improved sensing performance in comparison with Pt/rGO paper and commercial Pt foil electrode toward H_2O_2, and can been used for real-time tracking H_2O_2 secretion by live cells macrophages. Furthermore, it is worth to mention that our strategy for the preparation of free-standing Pt/rGO–CNT paper is expected to be a modular approach to fabricate other graphene-based paper with multi-functional components, which has a great potential for the development of high performance implantable biochemical devices, flexible energy conversion units, on-chip power sources, flexible lithium ion batteries, supercapacitor, and other electronic systems.

Acknowledgements

This work is supported by the National Natural Science Foundation of China (Grant 50773059) and the program of Nanyang Assistant Professorship of Nanyang Technological University, Singapore.

References

Chen, A., Holt-Hindle, P., 2010. Chem. Rev. 110, 3767–3804.

Chen, H., Müller, M. B., Gilmore, K. J., Wallace, G. G., Li, D., 2008. Adv. Mater. 20, 3557–3561.

Chen, K. J., Pillai, K. C., Rick, J., Pan, C. J., Wang, S. H., Liu, C. C., Hwang, B. J., 2012. Biosens. Bioelectron. 33, 120–127.

Chi, K., Zhang, Z., Xi, J., Huang, Y., Xiao, F., Wang, S., Liu, Y., ACS Appl. Mater. Interfaces in press.

Chuang, M. C., Yang, Y. L., Tseng, T. F., Chou, T., Lou, S. L., Wang, J., 2010. Talanta 81, 15–19.

Dikin, D. A., Stankovich, S., Zimney, E. J., Piner, R. D., Dommett, G. H. B., Evmenenko, G., Nguyen, S. T., Ruoff, R. S., 2007. Nature 448, 457–460.

Dong, S., Xi, J., Wu, Y., Liu, H., Fu, C., Liu, H., Xiao, F., Anal. Chim. Acta in press.

Endo, M., Muramatsu, H., Hayashi, T., Kim, Y. A., Terrones, M., Dresselhaus, N. S., 2005. Nature 433, 476–476.

Ensafi, A. A., Jafari-Asl, M., Rezaei, B., 2014. Electrochim. Acta 130, 397–405.

Gao, H., Wang, Y., Xiao, F., Ching, C. B., Duan, H., 2012. J. Phys. Chem. C 116, 7719–7725.

Guascito, M. R., Chirizzi, D., Malitesta, C., Mazzotta, E., Siciliano, M., Siciliano, T., Tepore, A., Turco, A., 2011. Biosens. Bioelectron. 26, 3562–3569.

Han, Y., Zheng, J., Dong, S., 2013. Electrochim. Acta 90, 35–43.

Hobbs, K. L., Larson, P. R., Lian, G. D., Keay, J. C., Johnson, M. B., 2004. Nano Lett. 4, 167–171.

Hu, Y., Li, X., Geng, D., Cai, M., Li, R., Sun, X., Zou, L., 2013. Electrochim. Acta 91, 227–233.

Hummers, W. S., Offeman, R. E., 1958. J. Am. Chem. Soc. 80, 1339–1339.

Ji, S., Guo, Q., Yue, Q., Wang, L., Wang, H., Zhao, J., Dong, R., Liu, J., Jia, J., 2011. Biosens. Bioelectron. 26, 2067–2073.

Kashem, M. M. A., Kaune, G., Diethert, A., Wang, W., Schlage, K., Couet, S., Röhlsberger, R., Roth, S. V., Müller-Buschbaum, P., 2011, Macromolecules 44, 1621–1627.

Lee, C., Wei, X. D., Kysar, J. W., Hone, J., 2008. Science 321, 385–388.

Li, Y. Q., Yu, T., Yang, T. Y., Zheng, L. X., Liao, K., 2012. Adv. Mater. 24, 3426–3431.

Liu, M., Liu, R., Chen, W., 2013. Biosens. Bioelectron. 45, 206–212

Miao, Y. E., He, S., Zhong, Y., Yang, Z., Tjiu, W. W., Liu, T., 2013. Electrochim. Acta 99, 117–123.

Nair, R. R., Blake, P., Grigorenko, A. N., Novoselov, K. S., Booth, T. J., Stauber, T., Peres, N. M. R., Geim, A. K., 2008. Science 320, 1308–1308.

Novoselov, K. S., Geim, A. K., Morozov, S. V., Jiang, D., Zhang, Y., Dubonos, S. V., Grigorieva, I. V., Firsov, A. A., 2004. Science 306, 666–669.

Oh, K. M., Cho, S. W., Kim, G. O., Ryu, K. S., Jeong, H. M., 2014. Electrochim. Acta 135, 478–486.

Park, S., An, J., Suk, J. W., Ruoff, R. S., 2010. Small 6, 210–212.

Pei, S., Zhao, J., Du, J., Ren, W., Cheng, H. M., 2010. Carbon 48, 4466–4474.

Seger, B., Kamat, P. V., 2009. J. Phys. Chem. C 113, 7990–7995.

Shakir, I., 2014. Electrochim. Acta 129, 396–400.

Suárez, G. Santschi, ,C., Martin, O. J. F., Slaveykova, V., 2013. Biosens. Bioelectron. 42, 385–390.

Sun, X., Guo, S., Liu, Y., Sun, S., 2012. Nano Lett. 12, 4859−4863.

Sun, Y., Wu, Q., Shi, G., 2011. Energy Environ. Sci. 4, 1113–1132.

Tang, Z., Shen, S., Zhuang, J., Wang, X., 2010. Angew. Chem. Int. Ed. 49, 4603–4607.

Wang, D. W., Li, F., Zhao, J., Ren, W., Chen, Z. G., Tan, J., Wu, Z. S., Gentle, I., Lu, G. Q., Cheng, H. M., 2009. ACS Nano 3, 1745–1752.

Wu, W. Y., Zhong, X., Wang, W., Miao, Q., Zhu, J. J., 2010. Electrochem. Commun. 12, 1600–1604.

Xi, F., Zhao, D., Wang, X., Chen, P., 2013. Electrochem. Commun. 26, 81–84.

Xiao, F., Song, J., Gao, H., Zan, X., Xu, R., Duan, H., 2012. ACS Nano 6, 100–110.

Xiao, F., Zhao, F., Zhang, Y., Guo, G., Zeng, B., J. Phys. Chem. C 2009, 113, 849–855.

Xu, F., Sun, Y., Zhang, Y., Shi, Y., Wen, Z., Li, Z., 2011. Electrochem. Commun. 13, 1131-1134

Yang, J., Zou, L., 2014. Electrochim. Acta 130, 791–799.

You, T., Niwa, O., Horiuchi, T., Tomita, M., Iwasaki, Y., Ueno, Y., Hirono, S., 2002. Chem. Mater. 14, 4796–4799.

Captions:

Fig. 1 Stress-strain curves of rGO–CNT paper and rGO paper. Insets are the optical photographs of rGO–CNT paper and rGO paper.

Fig. 2 Cross-sectional and top-sectional SEM images of rGO–CNT paper and rGO paper with different magnifications.

Fig. 3 Top-sectional SEM images of Pt/rGO–CNT paper and Pt/rGO paper with different magnifications.

Fig. 4 (A) CV curves of Pt/rGO–CNT, Pt/rGO, rGO–CNT and rGO paper electrodes in 0.1 M KCl containing 1.0 mM $K_3Fe(CN)_6$ and 1.0 mM $K_4Fe(CN)_6$. Scan rate: 20 mV s^{-1}. (B) CV curves of Pt/rGO–CNT paper, Pt/rGO paper and Pt foil electrodes in deaerated 0.5 M H_2SO_4. Scan rate: 50 mV s^{-1}. (C) Dependence of ECSA on the Pt content in Pt/rGO–CNT paper. Inset is the EDX spectrum of Pt/rGO–CNT paper. (D) Decrease of the ECSA during repeated potential cycling.

Fig. 5 (A) CV curves of Pt/rGO–CNT paper and Pt foil electrodes in 0.1 M PBS containing 1.0 mM H_2O_2. Scan rate: 50 mV s^{-1}. (B) Histograms of the current responses of Pt/rGO–CNT paper (a) and Pt foil (b) electrodes to 1.0 μM H_2O_2 in PBS at different applied potential. (C) Histograms of the current responses of Pt/rGO–CNT paper (a, b, c and d) and Pt/rGO paper (e, f, g and h) electrodes to 1.0 (a and e), 2.0 (b and f), 5.0 (c and g) and 10 μM (d and h) H_2O_2 in 0.1 M PBS. Applied potential: -0.05 V. Inset is the typical amperometric responses of Pt/rGO–CNT paper (a) and Pt/rGO paper (b) electrodes to 5.0 μM H_2O_2 in 0.1 M PBS. (D) Typical amperometric response of Pt/rGO–CNT paper electrode to successive addition of 0.1, 0.2, 0.5, 1.0 and 2.0 μM H_2O_2 in a stirring PBS. Inset is the amperometric response to successive addition of 10 nM H_2O_2. Applied potential: -0.05 V. (E) Corresponding calibration curves of panel C. (F) Effects of 180° bending times and bending angles on the

current response to 5.0 μM H_2O_2 using the flexible Pt/rGO–CNT paper electrode. And the current response of eight different Pt/rGO–CNT paper to 5.0 μM H_2O_2. The RSD is calculated from ten repeat measurements.

Fig. 6 (A) Bright-field image and (B) Dark-field image of live cells macrophages incubated with the Pt/rGO–CNT paper electrode for over 4 h. (C) Quantitative cell viability results using a standard cell counting Kit-8 assay. (D) Amperometric responses of Pt/rGO–CNT paper electrode in 0.1 M PBS (pH 7.4) with the addition of 0.1 mM PMA and 300 U mL^{-1} catalase in the presence (a) and absence (b) of macrophages. Applied potential: -0.05 V.

Highlights:

- Free-standing graphene–carbon nanotube paper serves as high-performance flexible and lightweight electrode.
- Ultrafine Pt nanoparticles are decorated on graphene–carbon nanotube paper by well controlled sputter deposition method.
- Pt nanoparticles decorated graphene–carbon nanotube paper electrode exhibits a variety of desirable electrochemical properties and good sensing performances.
- The resultant flexible biosensor has been used for the real-time tracking hydrogen peroxide secretion by live cells macrophages.

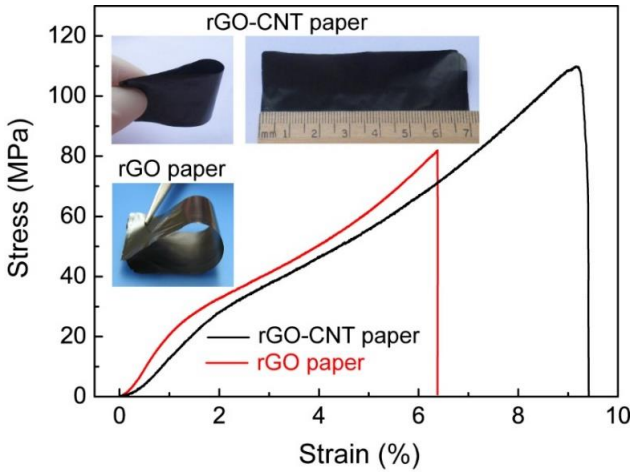

Figure 1

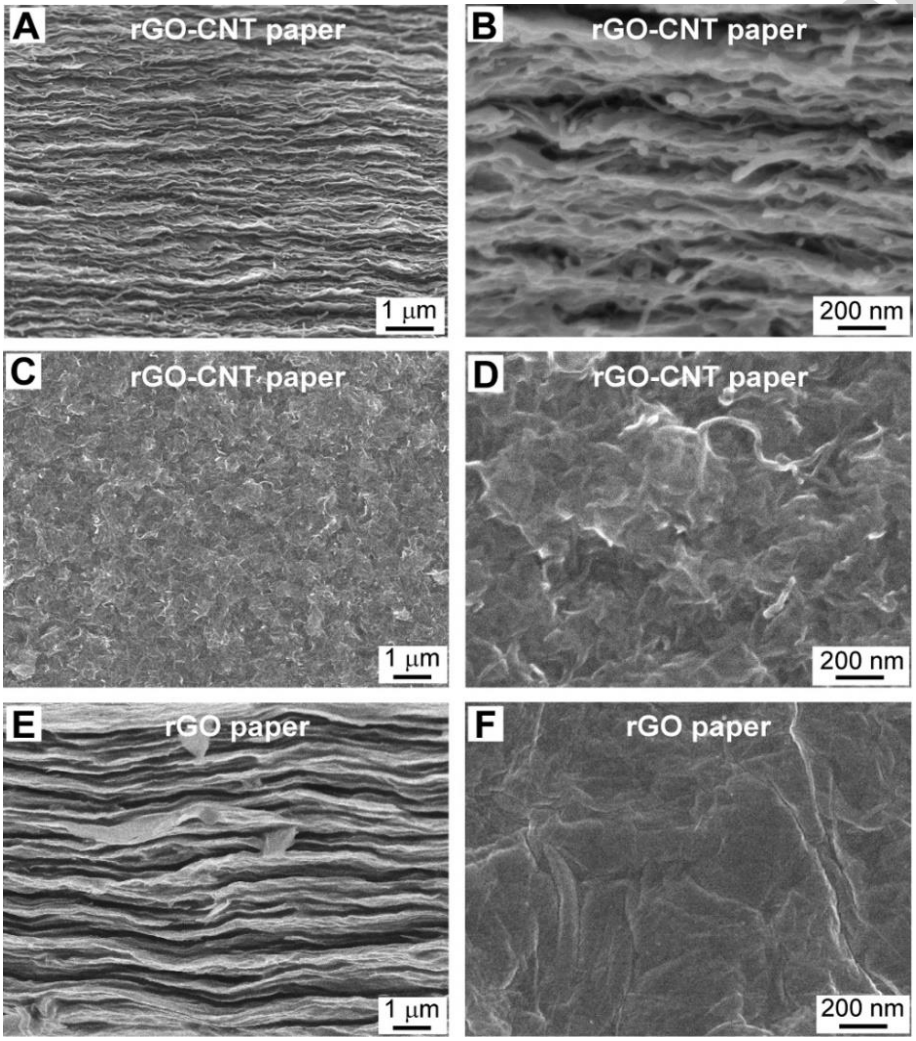

Figure 2

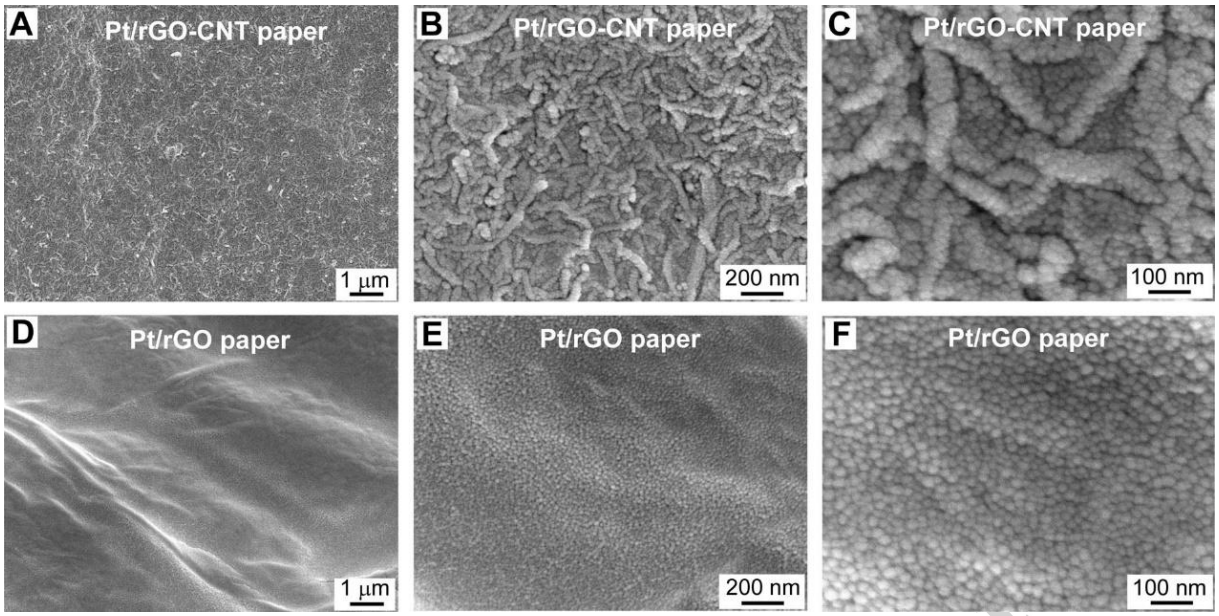

Figure 3

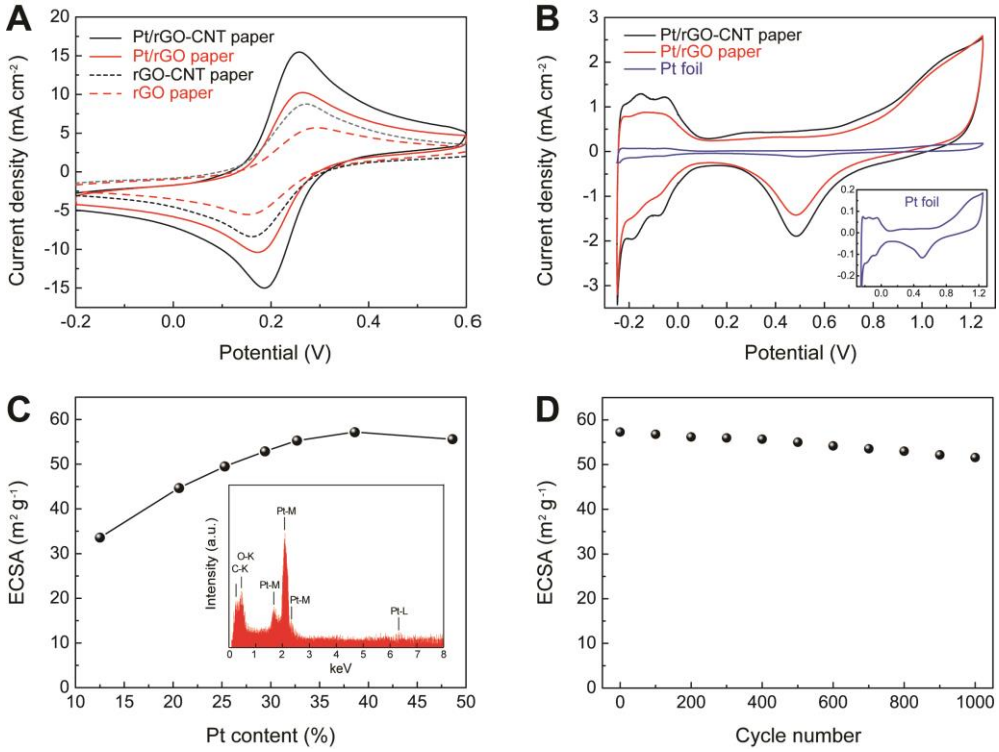

Figure 4

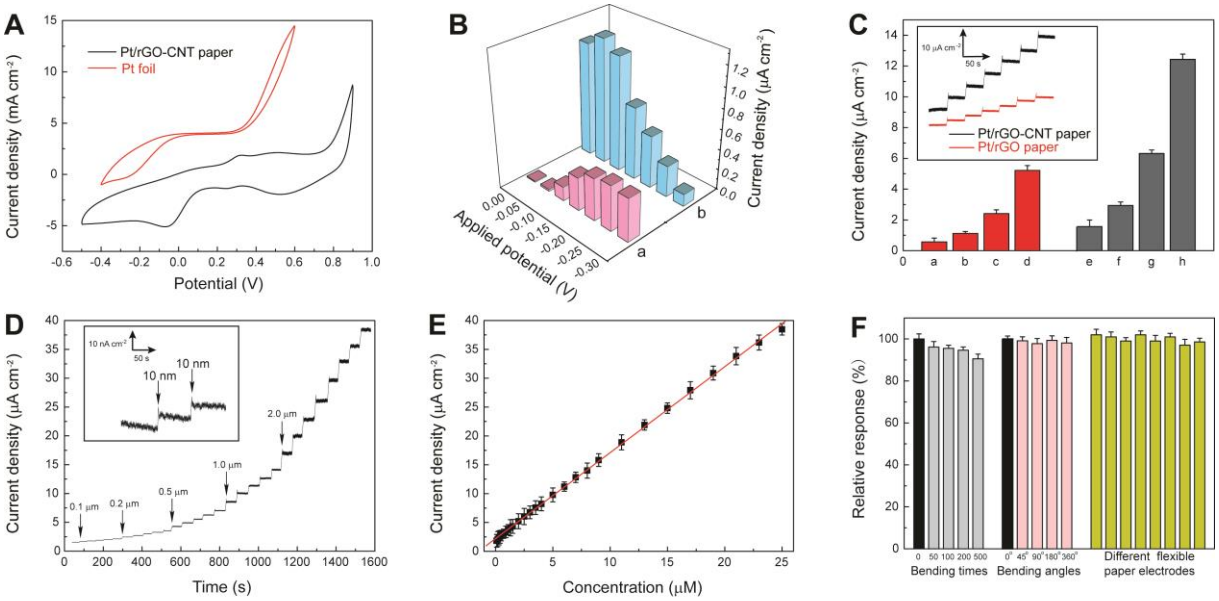

Figure 5

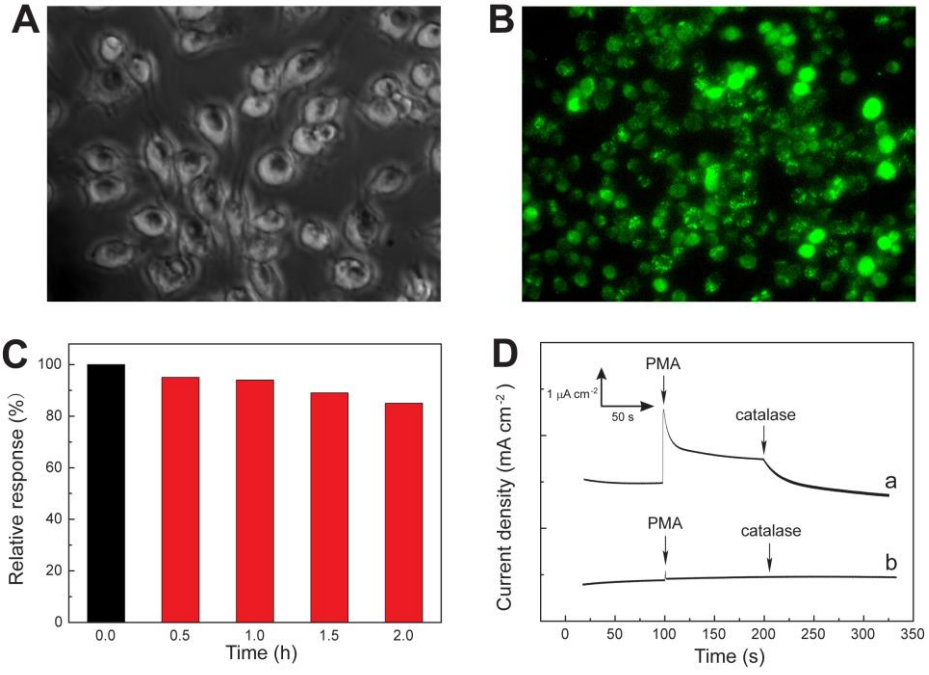

Figure 6